Oxidation of Histidine Residues in Copper-Zinc Superoxide Dismutase by Bicarbonate-Stimulated Peroxidase and Thiol Oxidase Activities: Pulse EPR and NMR Studies

ARTICLE *in* BIOCHEMISTRY · NOVEMBER 2010

Impact Factor: 3.02 · DOI: 10.1021/bi1010305 · Source: PubMed

6 AUTHORS, INCLUDING:

John Mccracken
Michigan State University
91 PUBLICATIONS **2,674** CITATIONS
SEE PROFILE

Francis C Peterson
Medical College of Wisconsin
107 PUBLICATIONS **2,416** CITATIONS
SEE PROFILE

Brian F Volkman
Medical College of Wisconsin
148 PUBLICATIONS **5,047** CITATIONS
SEE PROFILE

NIH Public Access
Author Manuscript
Biochemistry. Author manuscript; available in PMC 2012 November 19.

Published in final edited form as:
Biochemistry. 2010 December 21; 49(50): 10616–10622. doi:10.1021/bi1010305.

Oxidation of Histidine Residues in Copper-Zinc Superoxide Dismutase by Bicarbonate-Stimulated Peroxidase and Thiol Oxidase Activities: Pulse EPR and NMR Studies†

Karunakaran Chandran[1], **John McCracken**[2], **Francis C. Peterson**[3], **William E. Antholine**[1], **Brian F. Volkman**[3], and **Balaraman Kalyanaraman**[1,*]

[1]Department of Biophysics, Free Radical Research Center, Medical College of Wisconsin, Milwaukee, WI

[2]Department of Chemistry, Michigan State University, East Lansing, MI

[3]Department of Biochemistry, Medical College of Wisconsin, Milwaukee, WI

Abstract

In this work, we investigated the oxidative modification of histidine residues induced by peroxidase and thiol oxidase activities of bovine copper-zinc superoxide dismutase (Cu-ZnSOD) using NMR and pulse EPR spectroscopy. 1D NMR and 2D-NOESY were used to determine the oxidative damage at the Zn(II) and Cu(II) active sites as well as at distant histidines. Results indicate that during treatment of SOD with hydrogen peroxide (H_2O_2) or cysteine in the absence of bicarbonate anion (HCO_3^-), both exchangeable and non-exchangeable protons were affected. Both His-44 and His-46 in the Cu(II) active site were oxidized based on the disappearance of NOESY cross peaks between CH and NH resonances of the imidazole rings. In the Zn(II) site, only His-69, which is closer to His-44, was oxidatively modified. However, addition of HCO_3^- protected the active site His residues. Instead, resonances assigned to His-41 residue, 11 Å away from the Cu(II) site, were completely abolished during both HCO_3^- stimulated peroxidase activity and thiol oxidase activity in the presence of HCO_3^-. Additionally, ESEEM/HYSCORE and ENDOR studies of SOD treated with peroxide/Cys in the absence of HCO_3^- revealed that hyperfine couplings to the distal and directly coordinated nitrogens of the His-44 and His-46 ligands at the Cu(II) active site were modified. In the presence of HCO_3^-, these modifications were absent. HCO_3^- mediated, selective oxidative modification of histidines in SOD may be relevant to understanding the molecular mechanism of SOD peroxidase and thiol oxidase activities.

Cu, ZnSOD, a ubiquitous antioxidant enzyme present in the cytosol, nucleus, peroxisomes and mitochondrial intermembrane space of eukaryotic cells, protects against superoxide anion-dependent oxidative damage (1,2). The superoxide dismutase (SOD) activity is responsible for catalytically converting superoxide to hydrogen peroxide (3). In the presence of high concentration of H_2O_2, SOD is slowly inactivated ($k=3.1\ M^{-1}s^{-1}$) through formation of an active enzyme-bound oxidant, SOD-Cu(II)-$^{\bullet}$OH. The proposed mechanism for peroxidase activity is as follows (4–7).

†This work was supported by NIH Grants P41RR001008 and R01 NS040494.

*Department of Biophysics, Medical College of Wisconsin, 8701 Watertown Plank Road, Milwaukee, WI 53226 USA; 414-456-4000 (telephone); 414-456-6512 (fax); balarama@mcw.edu.

SUPPORTING INFORMATION AVAILABLE

Additional ESEEM spectra of SOD alone and treated with H_2O_2 are presented as supplementary materials. This material is available free of charge via the Internet at http://pubs.acs.org.

$$SOD{-}Cu(II){+}H_2O_2 \rightarrow SOD{-}Cu(I){+}O_2^{\cdot-}{+}2H^+ \quad \text{(Eq. 1)}$$

$$SOD{-}Cu(I){+}H_2O_2 \rightarrow SOD{-}Cu(II){-}{}^{\bullet}OH{+}OH^- \quad \text{(Eq. 2)}$$

The reactivity of the SOD-Cu(II)- $^{\bullet}OH$ was suggested to be similar to that of a "site-specific copper bound hydroxyl radical" (4–7). The inactivation of the enzyme was attributed to the oxidation of a histidine residue bound to the copper atom at the active site, forming an imidazole radical that underwent further oxidation to 2-oxo-histidine (8–10). The peroxidatic inactivation of SOD was mitigated by anionic, peroxidase substrates (formate, urate, azide, and nitrite) that have access to the active site of SOD, facilitated by the favorable electrostatic interaction (11–14).

Bicarbonate (HCO_3^-), a ubiquitous anion present in high concentrations (~25 mM) in biological systems stimulates SOD peroxidase activity. Proposed mechanisms (eqns. 1–3) suggest that HCO_3^- enters the active site of SOD through a narrow channel and undergoes oxidation at the active site in the presence of H_2O_2 or cysteine to form the carbonate anion radical, CO_3^-, that diffuses out of the active site and oxidizes other substrates in the bulk solution (11–14).

$$SOD{-}Cu(II){-}{}^{\bullet}OH{+}HCO_3^- \rightarrow SOD{-}Cu(II){+}CO_3^{\cdot-}{+}H_2O \quad \text{(Eq. 3)}$$

Using direct electron paramagnetic resonance (EPR) and electron nuclear double resonance (ENDOR) techniques, we have previously shown that the Cu(II) active site is not affected during HCO_3^--mediated enhanced peroxidase activity (15). More recently, it was shown that CO_2 is a potential reactant leading to the formation of CO_3^- during the peroxidase activity (17). In addition to the dismutase and peroxidase activities, SOD was also shown to autoxidize thiols in the presence of air to generate hydrogen peroxide *via* thiol oxidase activity (16).

To obtain a better understanding of the interaction between the histidine ligands and the oxidant generated at the active site of copper during HCO_3^- -stimulated SOD peroxidase/oxidase activities, we used NMR and pulse EPR spectroscopy techniques, electron spin echo envelope modulation (ESEEM) and hyperfine sublevel correlation (HYSCORE). Both 1D NMR and NOESY techniques were used to investigate the oxidative damage of histidines at the diamagnetic Zn(II) as well as the paramagnetic Cu(II) active site and at sites away from the coordination sphere of the active sites. ESEEM was used to determine the changes in the magnetic parameters of coordinated nitrogen (to active site copper and zinc) and distal nitrogens of both non-bridged and bridged histidine residues.

EXPERIMENTAL PROCEDURES (MATERIALS AND METHODS)

Materials

Bovine Cu-Zn SOD was obtained from Roche Diagnostics. Cysteine, deuterium oxide, hydrogen peroxide, sodium bicarbonate, sodium hydrogen phosphate and DTPA were purchased from Sigma (St. Louis, MO, USA).

NMR measurements

All ^{1}H-NMR experiments were performed on a Bruker 600 MHz spectrometer operating at 14.1 T. The solvent H_2O resonance was suppressed using a 3-9-19 watergate scheme (18). 2D-NOESY spectra were collected using a mixing time of 150 ms. The 2D experiments

were performed in phase-sensitive mode, using time-proportional phase-increment method. 512 free-induction decays were collected using the 2K data points. Data were multiplied by a phase-shifted squared sine bell along both dimensions. Zero filling in the f_1 dimension was applied to obtain a matrix of 2K × 1K data points.

Pulse EPR measurements

A typical reaction mixture (200 μl) for EPR measurements contained SOD (1.0 mM), H_2O_2 (5 mM), and HCO_3^- (50 mM) in a phosphate buffer (100 mM, pH 7.4) containing DTPA (100 μM). Incubation mixtures were then transferred to a 4 mm quartz EPR tube (Wilmad) and frozen immediately in liquid nitrogen for pulsed EPR analysis. Pulsed-EPR data were collected on a Bruker E-680X spectrometer operating at X-band and equipped with a model ER4118X-MD-4-W1 probe and employing a 4 mm dielectric resonator. The sample temperature was maintained at 10 K using an Oxford Instrument liquid helium flow system equipped with a CF-935 cryostat and an ITC-503 temperature controller. ESEEM data were collected using a three-pulse, stimulated echo sequence (90°-t-90°-T-90°) with 90° microwave pulse widths of 16 ns (full width at half-maximum) and peak powers of 250 W (19). A four-step phase cycling sequence, ($+x$, $+x$, $+x$), ($-x$, $+x$, $+x$), ($+x$, $-x$, $+x$), ($-x$, $-x$, $+x$), together with the appropriate addition and subtraction of the integrated spin echo intensities served to remove the contributions of two-pulse echoes and baseline offsets from the data. An integration window of 24 ns was used to acquire the spin echo amplitudes, using the data set length of 512 points. ESEEM data were tapered with a Hamming window and the Fourier-transformed ESEEM spectra were obtained by taking the absolute value of the Fourier transforms.

ENDOR measurements

The X-band ENDOR spectra were recorded on a Bruker E500 ELEXYS spectrometer using an ENDOR/triple accessory (Bruker) cavity. ENDOR spectra were recorded by fixing the magnetic field at an EPR resonance and by applying partially saturating microwave power while sweeping the NMR transition with radio frequency (RF) source. The samples were prepared as in pulsed EPR measurements.

^1H and ^{14}N ENDOR spectra were recorded at 8 K at the indicated field positions. The EPR spectrum was partially saturated with 6.33 mW (15 dB) of microwave power and the ENDOR spectra were recorded at 9.47 GHz with a 200 kHz modulation depth, 100 W radiofrequency power and 1300 scans at field position I and 4500 scans at field position III respectively.

Circular dichroism measurements

The CD spectra of SOD (10 μM) treated with H_2O_2 (100 μM) in the presence and absence of HCO_3^- (25 mM) were recorded on a Jasco 710 CD spectropolarimeter in 0.1-cm quartz cuvettes, accumulated eight times and corrected for the corresponding buffer using 1 nm band width.

RESULTS

NMR characterization of oxidized histidines during peroxidase and thiol oxidase activity of SOD: Protective effect of HCO_3^-

The changes in the histidine residues coordinated to copper (II) located at the active site and at distant sites during HCO_3^- -induced SOD peroxidase activity was investigated using NMR techniques. 1D NMR and ^1H-^1H NOESY spectra show the effect of H_2O_2/cysteine on histidine modification of SOD during peroxidase and thiol oxidase activities. The exchangeable N-H proton resonances observed by 1D NMR and the cross peaks between

both exchangeable and non-exchangeable protons of various histidines detected by 2D NMR (Fig. 1) were assigned according to Bertini *et al* (20).

During peroxidase activity in the absence of HCO_3^-, the signals became weaker and broadened due to conformational heterogeneity resulting from oxidative damage to active site histidines (Fig. 1B). In accordance with 1D NMR, the cross peaks between NH and CH protons of H44 (labeled as 3 & 4), H46 (labeled as 5 & 7) belonging to Cu(II) active site and H69 (labeled 1 & 2) of Zn(II) are altered (Fig. 1A&B). The oxidative damage of NH and CH protons of H44 residue in close proximity with H69 of Zn(II) possibly alters H-bond interaction between them. The H-bond between NH of H69 and CO of Thr-135 is important in stabilizing the active site channel (21). Thr-135 belongs to the six residue helix involved in the recognition and electrostatic guidance of the superoxide anion (21). However, in the presence of HCO_3^-, no significant changes occur to the Cu(II) active site histidine cross peaks (Fig. 1C). By contrast, in NOESY, the cross peak labeled 6 due to H41 of N-H & C2-H were also abolished (Fig. 1C, red circle with dashed lines). H41 (Hε2) is H-bonded to CO of Thr-39 (loop-III) and Hδ1 to CO of H120 (loop-VII) (22,23). The active site channel is formed by the electrostatic loop VII, where charged residues important in catalysis lie.

It has been reported that Cu, ZnSOD loses ~70 % of its catalytic activity upon disruption of the Thr39-His43-His120 hydrogen bridge by altering the positions and orientations of catalytically essential Leu-38 and Arg-143 residues (22,23). Both in the absence/presence of HCO_3^-, there is loss/reduction in Zn(II)-bound H69 cross peaks. The absence of changes in the circular dichroism (CD) spectra during peroxidase/thiol oxidase activities reveals that oxidative damage does not destabilize the SOD tertiary structure (Fig. 2). These findings suggest that HCO_3^- can protect SOD from oxidative damage at the active site by diverting the diffusible oxidant (e.g., CO_3^-) to a distant amino acid residue.

^{1}H-NMR and NOESY spectra of SOD during thiol oxidase activity in the absence of HCO_3^- is similar to those of control (Fig. 3). However, in the presence HCO_3^-, similar to that seen with SOD peroxidase activity, H41 cross peak labeled 6 was completely lost (Fig. 3). Also, the 1D peaks '*b*' and '*d*' characteristic of H41 were abolished (Fig. 3). The absence of oxidative damage in the absence of HCO_3^- during thiol oxidase activity may be due to slow reaction of H_2O_2 with Cys (24). However, in the presence of HCO_3^-, thiol oxidase activity stimulated SOD peroxidase activity leading to oxidative damage of other His residues.

ESEEM probing of histidines coordinated to copper site

^{14}N-ESEEM spectra of SOD are typical of the remote nitrogens of histidyl imidazole ligands strongly bound to Cu(II). Figure 4A shows 3-pulse time domain ESEEM data collected at g=2.06 for SOD (black trace), SOD treated with H_2O_2 (red trace) and SOD treated with H_2O_2 in the presence of bicarbonate (green trace). The 1D-ESEEM spectrum for SOD is typical for ^{14}N near the exact cancellation condition showing sharp peaks at 0.6, 1.0, 1.3, and 1.6 MHz, and a broader contribution with maxima at 4.1 and 4.5 MHz (Fig. S1). The 4-pulse HYSCORE spectrum for SOD (Fig. 4B) is characterized by two sets of strong cross peaks between ^{14}N double quantum (dq-dq) transitions centered at (1.3, 4.0 MHz) and (1.6, 4.4 MHz) (25,26). Minor correlations between single quantum and combination frequencies with the double quantum transitions were also detected. These findings are in agreement with a previous ESEEM study of ^{15}N-labeled SOD where two sets of nitrogen couplings were assigned to the four histidyl imidazole ligands bound to Cu(II) (27). Based on the previous report (27) the stronger hyperfine coupling, represented by the (1.6, 4.4 MHz) correlation in our HYSCORE spectra, was assigned to H44 and H46, while the weaker coupling, represented by the (1.3, 4.0 MHz) correlation, was assigned to H61 and H118.

ESEEM data collected for SOD treated with H_2O_2 show a 40% decrease in modulation depth (Fig 4A- red trace). Fourier transformation of these data show narrow peaks at 0.4, 1.3 and 1.6 MHz and a broad double quantum peak with an intensity maximum that stretches from about 3.8 to 4.2 MHz (Fig. S2). The corresponding HYSCORE spectrum (Fig. 4C) shows that the dominant ^{14}N dq-dq correlation is centered at (1.4,4.0 MHz) and extends over a frequency range from 3.5 to 4.3 MHz in the higher frequency dimension. A minor contribution at (1.5,4.4 MHz) is also detected (Fig. 4C). SOD samples treated with H_2O_2 in the presence of HCO_3^- showed three pulse ESEEM (Fig. 4A - green trace) and HYSCORE spectra (Fig. 4D) that were identical to those detected for untreated SOD (Fig. 4B).

Probing of copper-histidine coordination by ENDOR during SOD thiol oxidase activity

Proton ENDOR from histidines coordinated to Cu(II) were obtained at the field positions I, II, III indicated in Fig. 5 (*inset*). ^1H and ^{14}N ENDOR spectra of SOD during thiol oxidase activity in the absence of HCO_3^- reveal that resonances due to the coupled histidyl protons at the Cu(II) active site were broadened and diminished (Fig. 5). In contrast, the proton ENDOR spectra of SOD treated with cysteine in the presence of HCO_3^- were nearly similar to that of SOD alone. These results are in agreement with our earlier reports (15). Figure 5B shows the ^{14}N ENDOR spectra from histidines liganded to Cu(II) of SOD treated with cysteine alone and with HCO_3^-. The spectra for the field position I were simulated (Fig. 5B, *dotted line*) using the previously published parameters (28). Analysis of the spectra for the A_z direction revealed that there are two types of nitrogen signals, $N_z(1)$ His-44 and His-46 and $N_z(2)$ His-61 and His-118. However, the two values are overlapping at this orientation to give only a single set of lines, $N_z(1,2)$ (not shown). For the A_x direction, two sets of ^{14}N signals (Nx(1) and Nx(2)) were used in the simulation as shown in Figure 5B at field position III. These findings led us to conclude that the copper-bound His is not affected significantly in the presence of cysteine and HCO_3^-. However, in the presence of cysteine alone, the triplet signal in the low frequency region was considerably diminished (Fig. 5B at field position I). The triplet signal arises from His-44 and His-46 nitrogens (15). These results suggest that HCO_3^- -derived oxidant does not significantly alter the Cu(II) active site geometry and histidine coordination as does cysteine alone.

DISCUSSION

Nearly 35 years ago, Hodgson and Fridovich proposed that the reaction between H_2O_2 and SOD could generate a copper-bound hydroxyl radical (SOD-Cu(II)-$^{\bullet}$OH) that reacts with HCO_3^- to form a diffusible oxidant, CO_3^- that oxidized several peroxidatic substrates (ABTS, dichlorodihydrofluorescein, and others) outside of the active site (4,7,11–13). More recently, it was shown that CO_2, not HCO_3^-, undergoes peroxidation to CO_3^- in the presence of H_2O_2 and SOD (29). Using EPR spin-trapping methods, evidence for CO_3^- and other radicals derived from it was demonstrated during HCO_3^- -stimulated peroxidase activity of SOD (11,30). The oxidant derived from HCO_3^- (i.e., carbonate anion radical) was proposed to react with surface-associated Trp-32 in human SOD forming a tryptophanyl radical (31). Mutation of Trp-32 by phenylalanine totally eliminated the Trp-32 radical formed from hSOD reaction with H_2O_2 and HCO_3^- (31), providing additional evidence for the reaction between CO_3^- and tryptophan-32 on the surface of the protein (31).

An alternative mechanism for HCO_3^- -mediated peroxidase activity has also been proposed. It was proposed that the active species (peroxycarbonate or HCO_4^-) formed during the peroxidase activity is enzyme-associated and non-diffusible (32). It was also suggested that the enzyme-associated oxidant (HCO_4^-, a non-radical) does not diffuse away from the active site but reacts locally at the active site of copper-bound histidines. The present magnetic resonance analyses clearly rule out the “enzyme-bound peroxycarbonate” as an oxidant responsible for oxidation of the “distant” histidine residues. The mechanism of

direct oxidation of histidine at the active site by peroxycarbonate remains to be determined, however.

It was shown that SOD has a thiol oxidase activity (16). Previously, we proposed that HCO_3^- -stimulated peroxidase activity further accelerated thiol oxidase activity (24). Using a kinetic simulation model, the EPR profile changes in SOD-Cu(II) were simulated (24). Thiol oxidase activity generated *in situ* H_2O_2 needed for SOD peroxidase activity that was further stimulated by bicarbonate. The peroxidase activity enhanced thiol depletion and oxygen consumption resulting in increased thiol oxidase activity *via* formation of a diffusible CO_3^- species.

The ESEEM experiment offers a sensitive means for viewing the structural relationship between Cu(II) and its four coordinated histidine ligands (25, 26). In a HYSCORE experiment, the hyperfine coupling between Cu(II) and the remote nitrogen of a strongly bound histidyl imidazole ligand gives rise to cross peaks near (1.5, 4.0 MHz) whose contours are parallel to the frequency axes. The HYSCORE spectrum of SOD at g = 2.06 (Fig. 4B) shows two of these double quantum, dq-dq, cross peaks of nearly equal intensity that we can assign to a stronger set of hyperfine couplings due to H44 and H46, and a weaker set of couplings arising from H61 and H118 based on previous ESEEM studies (27). Treatment of the enzyme with H_2O_2 causes the ESEEM depth or amplitude to decrease by about 40% and the dq-dq correlation in the HYSCORE spectrum (Fig. 4C) is altered to show a more intense broader correlation centered at (1.4, 4.0 MHz) and a minor contribution at (1.6, 4.4 MHz). Previous studies of SOD treated with peroxide have shown that H118 is selectively oxidized to form a 2-oxo-histidine species (9). Although the ^{14}N-ESEEM amplitude is a function of the interplay between ligand hyperfine, nuclear Zeeman and nuclear quadrupole interactions, the HYSCORE spectra show that the hyperfine coupling changes that result from peroxide treatment are minor. The 40% loss in ESEEM amplitude can only be explained by the loss of at least one Cu(II)-histidine hyperfine interaction, commensurate with the breaking of the Cu(II) - H118 bond. This bond-breaking chemistry then leads to the changes in hyperfine coupling for the remaining histidyl imidazole ligands that are captured in the HYSCORE cross peak pattern centered at (1.4, 4.0 MHz). The previous biochemical studies that showed selective oxidation of H118, also showed that this modification only occurred in 66% of the Cu(II) sites. The residual cross peak due to the stronger Cu(II)-histidine interaction in H_2O_2 treated SOD (Fig. 4C) likely represents the fraction of Cu(II) sites where H118 is not oxidized and remains bound to Cu(II). Finally, the ESEEM data show conclusively that peroxide treatment in the presence of physiologically relevant levels of bicarbonate does not alter the ligation of H44, H46, H61 and H118 to Cu(II).

The present NMR study has limitations in that the 2D homonuclear NMR experiments using the commercially available protein enabled only the histidine analysis. The best way to confirm the structural assignments would have been to make recombinant SOD and the histidine mutants. To characterize the specific histidine modification, ^{15}N-labeled recombinant SOD should be used. Lack of these studies clearly present a limited scope for detailed experimental interpretations on the oxidative modification.

The present data using the combined approach involving ESEEM/HYSCORE, ENDOR, and 1D-NMR techniques are consistent with the previous mass spectral studies (9) indicating His118 oxidation during inactivation of Cu, Zn SOD with H_2O_2. The previous results also reported that histidine oxidation at other copper sites might be involved (9). The present magnetic resonance analyses also suggest marked changes in the hyperfine couplings at other copper(II)-histidine sites. These results reveal that the oxidation of His residues in Cu, Zn, SOD in the presence of H_2O_2 alone is presumably more extensive. However, the NMR

and ESEEM/HYSCORE results indicate that in the presence of bicarbonate the histidine oxidation is selective, occurring outside of the active site.

The present results are significant because HCO_3^- is abundant in all living cells protecting SOD from its oxidative damage at the active site but causes extensive damage to outer residues of SOD or other vital proteins as observed in neurodegenerative diseases. A large body of evidence indicates that elevated oxidative stress perhaps due to peroxidase/thiol oxidase stimulated peroxidase activity of SOD could play a major role in free radical biology. Finally, the combined use of NMR and EPR techniques is a powerful approach to elucidate the structural biological changes induced by site-specific generation of oxidants in biomolecules.

Summary

The combined NMR and pulse EPR data show that in the absence of HCO_3^-, the Cu(II) binding histidine residues were specifically oxidized and the other histidine residues were not affected during peroxidase and thiol oxidase activity of SOD. However, in the presence of HCO_3^-, the Cu(II) bound histidines in SOD were unaffected; instead, a distant histidine residue (Fig. 1D) was oxidized by a diffusible oxidant (most likely CO_3^-) formed at the active site of SOD.

Supplementary Material

Refer to Web version on PubMed Central for supplementary material.

Acknowledgments

C.K. expresses thanks to the Managing Board, VHNSN College, Virudhunagar, India for his sabbatical leave.

Abbreviations

2D-NOESY	Two-dimensional nuclear Overhauser effect spectroscopy
CD	circular dichroism
CO_3^-	carbonate radical anion
Cu-ZnSOD	copper-zinc superoxide dismutase
ENDOR	electron nuclear double resonance
EPR	electron paramagnetic resonance
ESEEM	electron spin echo envelope modulation
H_2O_2	hydrogen peroxide
HCO_3^-	bicarbonate anion
HYSCORE	hyperfine sublevel correlation
SOD	superoxide dismutase

References

1. McCord JM, Fridovich I. Superoxide dismutase. An enzymic function for erythrocuprein (hemocuprein). J Biol Chem. 1969; 244:6049–6055. [PubMed: 5389100]
2. Okado-Matsumoto A, Fridovich I. Subcellular distribution of superoxide dismutases (SOD) in rat liver: Cu, Zn-SOD in mitochondria. J Biol Chem. 2001; 276:38388–38393. [PubMed: 11507097]

3. McCord JM, Fridovich I. The reduction of cytochrome c by milk xanthine oxidase. J Biol Chem. 1968; 243:5753–5760. [PubMed: 4972775]

4. Fridovich I. Suproxide dismutases. Annu Rev Biochem. 1975; 44:147–159. [PubMed: 1094908]

5. Fridovich I. Superoxide radical and superoxide dismutases. Annu Rev Biochem. 1995; 64:97–112. [PubMed: 7574505]

6. Hodgson EK, Fridovich I. The interaction of bovine erythrocyte superoxide dismutase with hydrogen peroxide: chemiluminescence and peroxidation. Biochemistry. 1975; 14:5299–5303. [PubMed: 172122]

7. Hodgson EK, Fridovich I. The interaction of bovine erythrocyte superoxide dismutase with hydrogen peroxide: inactivation of the enzyme. Biochemistry. 1975; 14:5294–5298. [PubMed: 49]

8. Sato K, Akaike T, Kohno M, Ando M, Maeda H. Hydroxyl radical production by H_2O_2 plus Cu, Zn-superoxide dismutase reflects the activity of free copper released from the oxidatively damaged enzyme. J Biol Chem. 1992; 267:25371–25377. [PubMed: 1334093]

9. Uchida K, Kawakishi S. Identification of oxidized histidine generated at the active site of Cu, Zn-superoxide dismutase exposed to H_2O_2 Selective generation of 2-oxo-histidine at the histidine 118. J Biol Chem. 1994; 269:2405–2410. [PubMed: 8300566]

10. Uchida K, Kawakishi S. Site-specific oxidation of angiotensin I by copper(II) and L-ascorbate: conversion of histidine residues to 2-imidazolones. Arch Biochem Biophys. 1990; 283:20–26. [PubMed: 2241171]

11. Zhang H, Joseph J, Gurney M, Becker D, Kalyanaraman B. Bicarbonate enhances peroxidase activity of Cu, Zn-superoxide dismutase. J Biol Chem. 2002; 277:1013–1020. [PubMed: 11682485]

12. Singh RJ, Goss SPA, Joseph J, Kalyanaraman B. Nitration of γ-tocopherol and oxidation of α-tocopherol by copper-zinc superoxide dismutase/H_2O_2/NO_2-: role of nitrogen dioxide free radical. Proc Natl Acad Sci USA. 1998; 95:12912–12917. [PubMed: 9789014]

13. Andrekopoulos C, Zhang H, Joseph J, Kalivendi S, Kalyanaraman B. Bicarbonate enhances α-synuclein oligomerization and nitration: intermediacy of carbonate radical anion and nitrogen dioxide radical. Biochem J. 2004; 378:435–447. [PubMed: 14640973]

14. Sankarapandi S, Zweier JL. Bicarbonate is required for the peroxidase function of Cu, Zn-superoxide dismutase at physiologic pH. J Biol Chem. 1999; 274:1226–1232. [PubMed: 9880490]

15. Karunakaran C, Zhang H, Crow JP, Antholine WA, Kalyanaraman B. Direct probing of copper active site and free radical formed during bicarbonate-dependent peroxidase activity of bovine and human copper, zinc superoxide dismutases: Low-temperature electron paramagnetic resonance and electron nuclear double resonance studies. J Biol Chem. 2004; 279:32534–32540. [PubMed: 15123612]

16. Winterbourn CC, Peskin AV, Parsons-Mair HN. Thiol oxidase activity of copper, zinc superoxide dismutase. J Biol Chem. 2002; 277:1906–1911. [PubMed: 11698397]

17. Liochev SI, Fridovich I. Mechanism of the peroxidase activity of Cu, Zn superoxide dismutase. Free Radic Biol Med. 2010; 48:1565–1569. [PubMed: 20211248]

18. Sklenar V, Piotto M, Leppik R, Saudek V. Gradient-tailored water suppression for ^{1}H-^{15}N HSQC experiments optimized to retain full sensitivity. J Magn Reson Series A. 1993; 102:241–245.

19. Sharpe MA, Krzyaniak MD, Xu S, McCracken J, Ferguson-Miller S. EPR evidence of cyanide binding to the Mn(Mg) center of cytochrome c oxidase: Support for Cu(A)-Mg involvement in proton pumping. Biochemistry. 2009; 48:328–335. [PubMed: 19108635]

20. Bertini I, Capozzi F, Luchinat C, Piccioli M, Viezzoli MS. Assignment of active-site protons in the 1H-NMR spectrum of reduced human Cu/Zn superoxide dismutase. Eur J Biochem. 1991; 197:691–697. [PubMed: 1851482]

21. Tainer JA, Getzoff ED, Richardson JS, Richardson DC. Structure and mechanism of copper, zinc superoxide dismutase. Nature. 1983; 306:284–287. [PubMed: 6316150]

22. Shipp EL, Cantini F, Bertini I, Valentine JS, Banci L. Dynamic properties of the G93A mutant of copper-zinc superoxide dismutase as detected by NMR spectroscopy: implications for the pathology of familial amyotrophic lateral sclerosis. Biochemistry. 2003; 42:1890–1899. [PubMed: 12590575]

23. Toyama A, Takahashi Y, Takeuchi H. Catalytic and structural role of a metal-free histidine residue in bovine Cu-Zn superoxide dismutase. Biochemistry. 2004; 43:4670–4679. [PubMed: 15096035]
24. Karunakaran C, Zhang H, Joseph J, Antholine WE, Kalyanaraman B. Thiol oxidase activity of copper, zinc superoxide dismutase stimulates bicarbonate-dependent peroxidase activity via formation of a carbonate radical. Chem Res Toxicol. 2005; 18:494–500. [PubMed: 15777089]
25. Mims WB, Peisach J. The nuclear modulation effect in electron spin echos for complexes of Cu^{+2} and imidazole with 14N and 15N. J Chem Phys. 1978; 69:4921–4930.
26. Kofman V, Farver O, Pecht I, Goldfarb D. Two-dimensional pulsed EPR spectroscopy of the copper protein azurin. J Am Chem Soc. 1996; 118:1201–1206.
27. Dikanov S, Felli I, Viezzoli MS, Spoyalov A, Hüttermann J. X-band ESEEM spectroscopy of 15N substituted native and inhibitor-bound superoxide dismutase. Hyperfine couplings with remote nitrogen of histidine ligands. FEBS Lett. 1994; 345:55–60. [PubMed: 8194601]
28. Reinhard H, Kappl R, Hütterman J, Viezzoli MS. ENDOR of superoxide dismutase: structure determination of the copper site from randomly oriented specimen. J Phys Chem. 1994; 98:8806–8812.
29. Liochev SI, Fridovich I. CO_2, not HCO_3^-, facilitates oxidations by Cu, Zn superoxide dismutase plus H_2O_2. Proc Natl Acad Sci USA. 2004; 101:743–744. [PubMed: 14711995]
30. Ramirez DC, Gomez Mejiba SE, Mason RP. Mechanism of hydrogen peroxide-induced Cu, Zn-superoxide dismutase-centered radical formation as explored by immune-spin trapping: the role of copper- and carbonate radical anion-mediated oxidations. Free Radic Biol Med. 2005; 38:201–214. [PubMed: 15607903]
31. Zhang H, Andrekopoulos C, Joseph J, Karunakaran C, Karoui H, Crow JP, Kalyanaraman B. Bicarbonate-dependent peroxidase activity of human Cu, Zn-superoxide dismutase induces covalent aggregation of protein: intermediacy of tryptophan-derived oxidation products. J Biol Chem. 2003; 278:24078–24089. [PubMed: 12686560]
32. Elam JS, Malek K, Rodriguez JA, Doucette PA, Taylor AB, Hayward LJ, Cabelli DE, Valentine JS, Hart PJ. An alternative mechanism of bicarbonate-mediated peroxidation by copper-zinc superoxide dismutase: rates enhanced via proposed enzyme-associated peroxycarbonate intermediate. J Biol Chem. 2003; 278:21032–21039. [PubMed: 12649272]

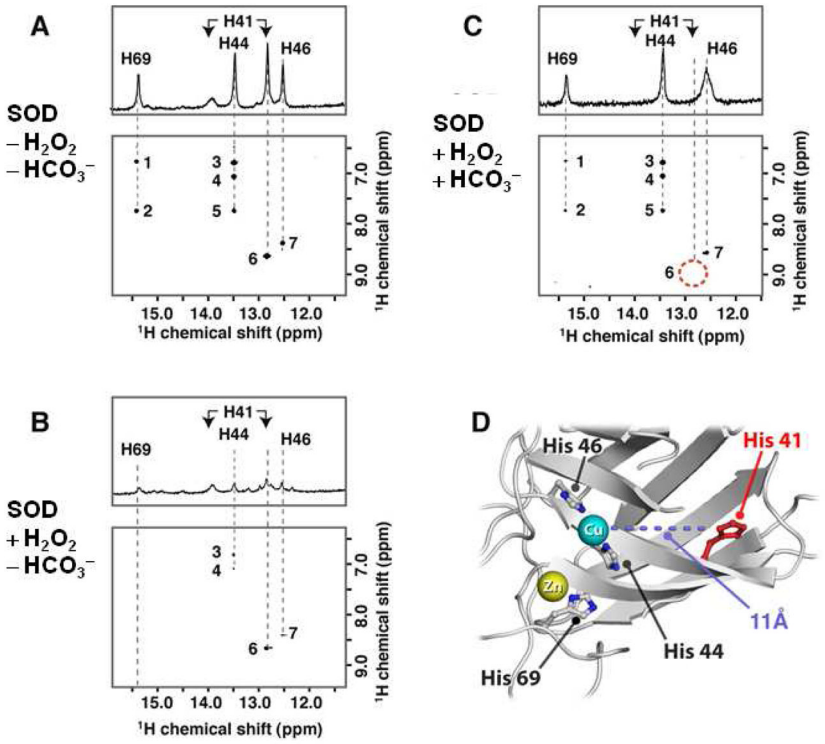

Figure 1.

The effect of HCO_3^- on oxidation of histidinyl residues of SOD: NMR studies. (A) 600 MHz ^1H-^1H NOESY and 1D NMR (as inset) spectra in H_2O of SOD (1 mM) in 20 mM phosphate buffer (pH 7.4). (B) Same as (A) but in the presence of H_2O_2 (3 mM). (C) Same as (B) but in the presence of HCO_3^- (50 mM). The labeled cross-peaks and 1D peaks are as follows: 1, H69 N-H & C4-H; 2, H69 N-H & C2-H; 3, H44 N-H & C2-H; 4, H44 N-H & C4-H; 5, H46 N-H & H69 C2-H; 6, H41 N-H & C2-H; 7, H46 N-H & C2-H and *a*, H46; *b*, H41; *c*, H44; *d*, H41(H3); *e*, H69. (D) Ribbon diagram of SOD (PDB ID 2SOD) showing the His-41 side chain oxidized in the presence of HCO_3^- in red and active site His residues oxidized in the absence of HCO_3^- in gray.

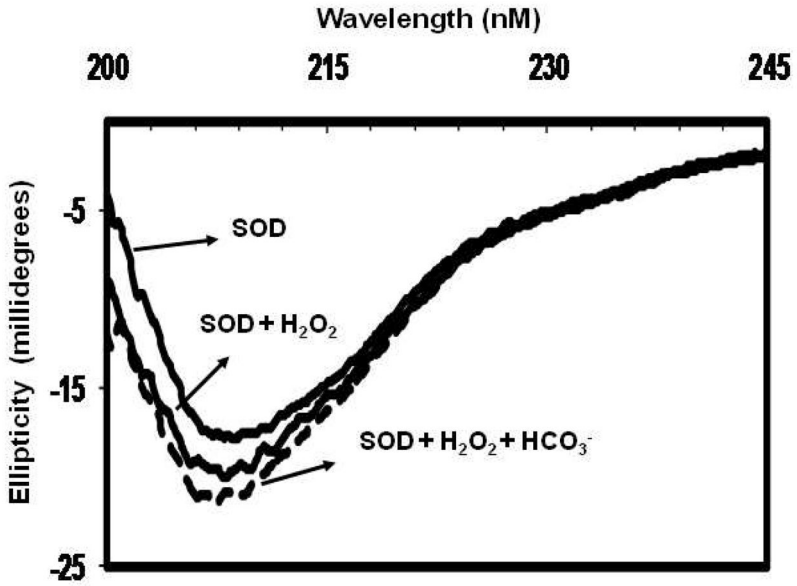

Figure 2.
The CD spectra of SOD (10 μM) treated with H_2O_2 (100 μM) in the presence and absence of HCO_3^- (25 mM) in phosphate buffer (50 mM, pH 7.4) containing DTPA (100 μM).

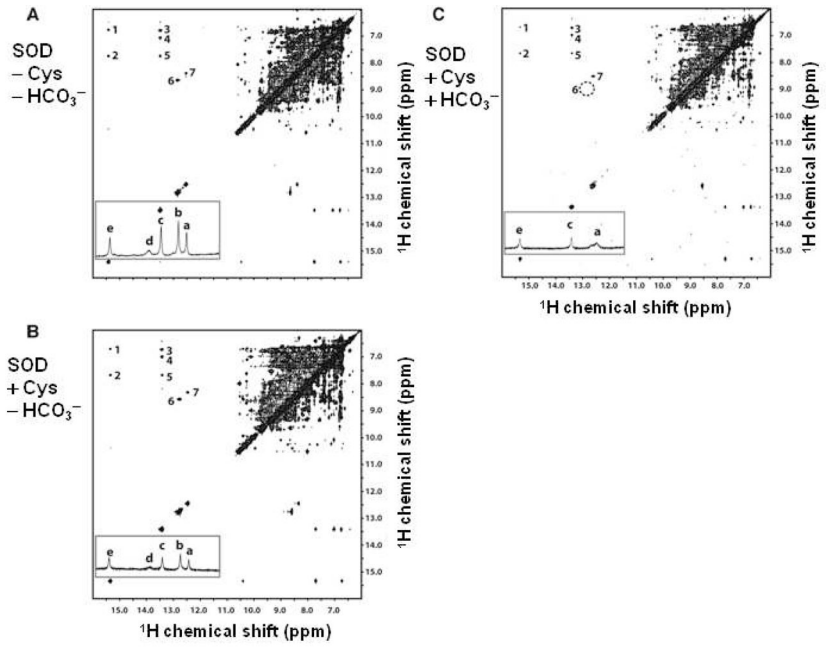

Figure 3.

(A) 600 MHz ^{1}H-^{1}H NOESY and 1D NMR (as inset) spectra in 90% H_2O and 10% D_2O of Cu, Zn-SOD (1 mM) in 20 mM phosphate buffer (pH 7.4). (B) Same as (A) but incubated with cysteine (500 μM). (C) Same as (B) but incubated in presence of HCO_3^- (50 mM) for 4 hr. It was then followed by reduction of Cu(II) with 3 mM cysteine. Spectrometer conditions are described in the Materials and Methods section. The cross-peaks and 1D peaks are labeled as follows: 1, H69 N-H & C4-H; 2, H69 N-H & C2-H; 3, H44 N-H & C2-H; 4, H44 N-H & C4-H; 5, H46 N-H & H69 C2-H; 6, H41 N-H & C2-H; 7, H46 N-H & C2-H and *a*, H46; *b*, H41; *c*, H44; *d*, H41(H3); *e*, H69.

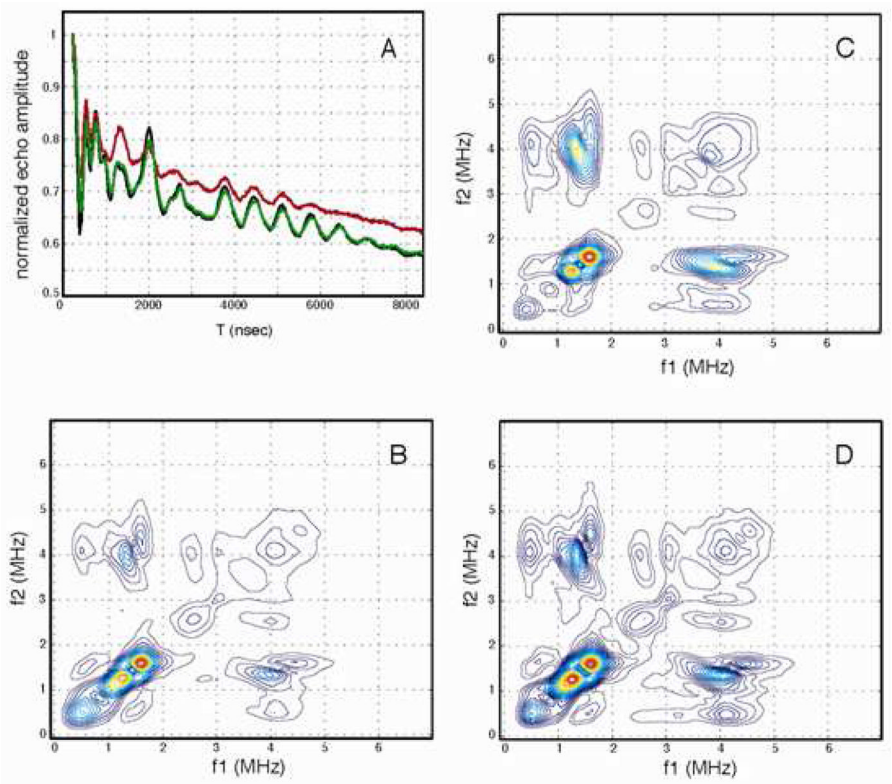

Figure 4.

Three pulse time domain ESEEM spectra (A) and 4-pulse HYSCORE spectra collected for SOD in H2O in 100 mM phosphate buffer, pH=7.4 (B), SOD treated with H_2O_2 (C), and SOD treated with H_2O_2 in the presence of HCO_3^- (D). For (A), the black and green traces were collected for SOD and the SOD treated with H_2O_2 in the presence of HCO_3^-, respectively, while the red trace was collected for the SOD sample treated with H_2O_2. Conditions for data acquisition common to all data sets were: microwave frequency, 9.681 GHz, magnetic field strength, 335.0 mT; tau value, 140 ns; sample temperature, 10K. Pulse powers of equal amplitude were used for HYSCORE data acquisition.

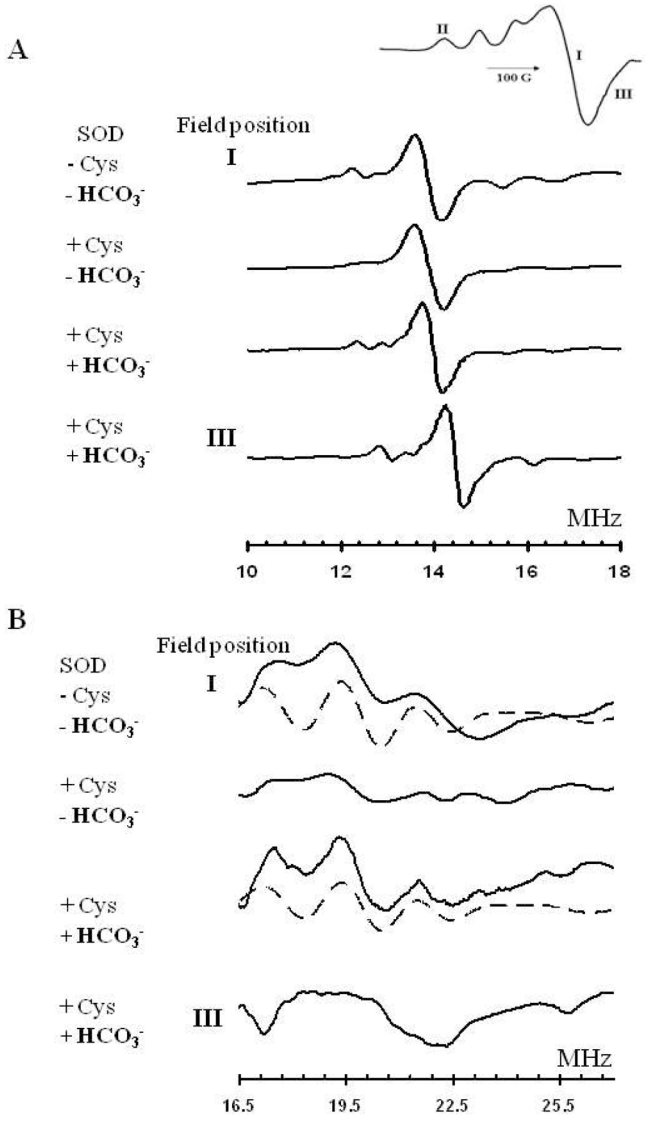

Figure 5.

(A) The X-band ^{1}H ENDOR and (B) ^{14}N ENDOR of SOD in the presence of cysteine (cys) and or HCO_3^- at indicated field positions I and III of EPR spectrum of SOD (inset). The SOD (1 mM) was incubated with cysteine (500 μM) for 4 h and repeated for 5 more times to equilibrate the cysteine concentration, 3 mM in 100 mM phosphate buffer, pH 7.4 with or without HCO_3^- (50 mM) containing 100 μM DTPA at 8 K. Spectrometer conditions are described for the ENDOR measurements in the Methods section.